Chapter 2
Classical Cross Section

2.1 Deflection Function

The question whether physical phenomena can be described "classically" or need a microscopic treatment, i.e. need quantum mechanics for their description is fundamental and still under intensive discussion. Ever larger objects (e.g. heavy ions, see below in Sect. 3.4, large molecules like the fullerenes) have been shown to have quantum properties. They exhibit e.g. interference. This touches upon basic concepts such as *Schrödinger's Cat* or *decoherence* of quantum states by the environment. For our purpose it may suffice to assume a fundamentally quantum-mechanical description that in special cases, i.e. when the relevant de Broglie wavelengths are small, may be approximated by classical methods.

Cross sections are the central observable of nuclear and particle physics. In some areas of nuclear physics (e.g. heavy-ion physics) nuclear reactions (scattering) are often treated semi-classically. Likewise, the historically important Rutherford scattering can be treated classically. The classical description implies that particles and their trajectories are localized. However, in each case it must be checked whether a classical description is valid. A criterion for classicity is (like in geometrical light optics) the wavelength of the radiation used is small as compared with some characteristic object dimension d. In agreement with Heisenberg's uncertainty relation this means

$$\lambda\!\!\!^{-}_{\text{deBroglie}} = \hbar/p \ll d. \tag{2.1}$$

When choosing for a typical object dimension half the distance of the trajectory turning point d_0 for a central collision the Sommerfeld criterion for classical scattering is obtained (with $\alpha = e^2/\hbar c$ Sommerfeld's fine-structure constant and β a short notation for v/c)

$$\eta_S = \frac{Z_1 Z_2 e^2}{\hbar v} = Z_1 Z_2 \frac{e^2}{\hbar c} \cdot \frac{c}{v} = Z_1 Z_2 \cdot \frac{\alpha}{\beta} \gg 1 \tag{2.2}$$

H. Paetz gen. Schieck, *Nuclear Reactions*, Lecture Notes in Physics 882,
DOI 10.1007/978-3-642-53986-2_2,

or numerically (for a very heavy target, thus at rest in the c.m. system)

$$\eta_S \approx 0.16 \cdot Z_1 Z_2 \sqrt{\frac{A_{\text{proj}}}{E_{\text{lab}}(\text{MeV})}} \gg 1 \tag{2.3}$$

with A_{proj} and E_{lab} the projectile mass number and its kinetic energy in the lab. system, respectively.

There exist more refined criteria, which take into account that the wave nature of the radiation leads to diffraction phenomena, especially where the scattering potential changes strongly, e.g. at the nuclear surface. Therefore, a requirement is postulated that the de Broglie wavelength not change substantially by the potential gradient. For Coulomb scattering this provides a scattering-angle dependent criterion [NOE76]

$$\eta_S^2 \gg \eta_{\text{crit}}^2 = \left[\frac{\sin^2 \frac{\theta}{2}}{\cos \frac{\theta}{2}(1 - \sin \frac{\theta}{2})}\right]^2. \tag{2.4}$$

Thus, a classical description is always possible at $\theta = 0°$ but never at $\theta = 180°$.

In the case of scattering of identical particles exchange symmetry and its ensuing interference effects entirely forbid any classical description (see below).

Here we present a complete definition of the (classical) cross section, which can be easily translated into a quantum-mechanical definition.

Definition of "Cross Section" The (differential) cross section is the number of particles of a given type from a reaction, which, per target atom and unit time, are scattered into the solid-angle element $d\Omega$ (formed by the angular interval $\theta \ldots \theta + d\theta$ and $\phi \ldots \phi + d\phi$), divided by the incident particle flux j (a current density = number of particles passing a unit area per unit time).

In the following we assume azimuthal (i.e. ϕ) independence of the scattering (e.g. valid for particles without spins or particles with spins, but with spin-independent interactions). The classical scattering situation is characterized by a definite trajectory and a unique relation between each particle incident from $r \to -\infty$ at a definite perpendicular distance b (the *impact parameter*) from the z axis and its (asymptotic) scattering angle at $r \to +\infty$ after the interaction. This definition yields the classical formula for the cross section. With the number of particles per unit time $j d\sigma = j \cdot 2\pi b db$ one obtains

$$\left(\frac{d\sigma}{d\Omega}\right)_{\text{class}} = \frac{2\pi b db}{2\pi \sin\theta d\theta} = \frac{b}{\sin\theta} \cdot \left|\frac{db}{d\theta}\right|. \tag{2.5}$$

$b = b(\theta, E)$ contains the influence of the interaction (the dynamics). $\theta(b)$ for obvious reasons is called *deflection function*. Its knowledge determines the scattering completely.

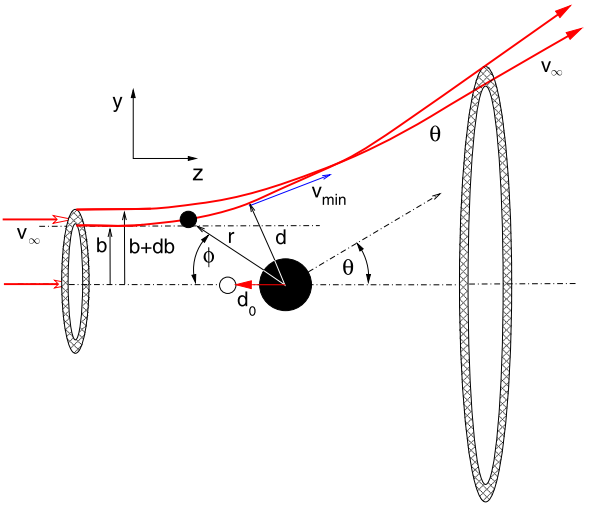

Fig. 2.1 Classical Rutherford scattering. b is the *impact parameter*, (r, ϕ) are the polar coordinates of the projectile, θ the polar scattering angle, d is the distance of closest approach, and d_0 its minimum for a central collision

2.2 Rutherford Scattering

2.2.1 Rutherford Scattering Cross Section

The situation for the case of Rutherford scattering (for a repulsive Coulomb force between equal charges) is shown in Fig. 2.1. For the derivation of the Rutherford scattering cross section we assume:

- The projectile and the scattering center (target) are point particles (with Gauss's law it can be proved that this is also fulfilled for extended particles as long as the charge distribution is not touched upon).
- The target nucleus is infinitely heavy (i.e. the laboratory system coincides with the c.m. system).[1]
- The interaction is the purely electrostatic Coulomb force (more precisely: the monopole term of this force)[2]

$$F_C = \pm \frac{1}{4\pi\epsilon_0} \cdot \frac{Z_1 Z_2 e^2}{r^2} = \frac{C}{r^2} \tag{2.6}$$

with the Coulomb potential $V_C = \pm C/r$.

The deflection function is most simply determined by applying angular-momentum conservation and the equation of motion in one coordinate (y) (v_∞, E_∞, and

[1] In all scattering/reaction problems the projectile mass $m = m_a$ is correct for an infinitely heavy target or in the lab. system of coordinates with the target (mass m_A) at rest. In the c.m. system used for theoretical considerations m has to be understood as the *reduced mass* $\mu = m_a m_A/(m_a + m_A)$.

[2] The term $1/4\pi\epsilon_0$ is correct in SI units. Throughout the remainder of this book—as usual in the nuclear physics literature—it is set equal to 1 (Gaussian system of units).

p_∞ are the asymptotic (i.e. valid or prepared at $r \to \pm\infty$) quantities: projectile velocity, kinetic energy, and momentum).

$$L = mv_\infty b = mr^2\dot{\phi} = mv_{\min}d \tag{2.7}$$

and from this

$$dt = r^2 d\phi / v_\infty b \tag{2.8}$$

$$\begin{aligned} m\Delta v_y &= \int F_y dt \\ v_\infty \sin\theta &= \frac{C}{mv_\infty b}\int_{-\infty}^{\infty} \dot{\phi}\sin\phi dt \\ &= \frac{C}{mv_\infty b}\int_0^{\pi-\theta} \sin\phi d\phi = \frac{C}{mv_\infty b}(1+\cos\theta). \end{aligned} \tag{2.9}$$

After transformation to half the scattering angle the deflection function is

$$\cot(\theta/2) = mv_\infty^2 b/C = v_\infty L/C \tag{2.10}$$

and

$$b = \frac{C}{2E_\infty}\cdot\cot\left(\frac{\theta}{2}\right) \tag{2.11}$$

and

$$\frac{db}{d\theta} = \frac{C}{2mv_\infty^2}\cdot\frac{1}{\sin^2(\theta/2)} = \frac{C}{4E_\infty}\cdot\frac{1}{\sin^2(\theta/2)} \tag{2.12}$$

and thus for the Rutherford cross section

$$\frac{d\sigma}{d\Omega} = \left(\frac{Z_1 Z_2 e^2}{4E_\infty}\right)^2 \cdot \frac{1}{\sin^4(\theta/2)}. \tag{2.13}$$

Numerically:

$$\frac{d\sigma}{d\Omega} = 1.296\left(\frac{Z_1 Z_2}{E_\infty(\text{MeV})}\right)^2 \cdot \frac{1}{\sin^4(\theta/2)}\left[\frac{mb}{sr}\right]. \tag{2.14}$$

Figure 2.2 shows the strong angle dependence of this cross section together with the original data of Ref. [GEI13], adjusted to the theoretical curve shown.

2.2.2 *Minimal Scattering Distance d*

For this quantity one needs additionally the energy-conservation law:

$$\frac{mv_\infty^2}{2} = \frac{mv_{\min}^2}{2} + \frac{C}{d}. \tag{2.15}$$

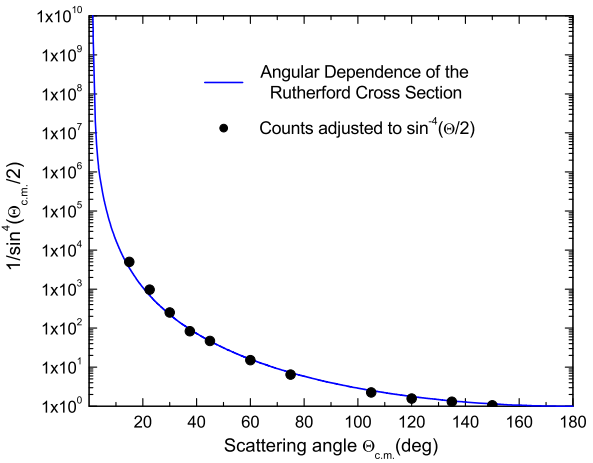

Fig. 2.2 The *curve* shows the angular dependence of the theoretical Rutherford cross section $\propto \sin^{-4}(\theta/2)$. The *points* are the original data (that consisted of tabulated numbers of counts with no error bars, and not transformed into cross-section values) of Ref. [GEI13], adjusted to the theoretical curve, giving a nearly perfect fit (Nowadays data with at least an error estimate or, better, error bars are mandatory)

The absolutely smallest distance d_0 is obtained in central collisions with:

$$E_\infty = \frac{m v_\infty^2}{2} = \frac{C}{d_0}. \tag{2.16}$$

From this and the angular-momentum conservation Eq. (2.7) the relation

$$b^2 = d(d - d_0) \tag{2.17}$$

is obtained with the solution:

$$\begin{aligned} d &= \frac{C}{2E_\infty}\left(1 + \sqrt{1 + b^2 \frac{4E_\infty^2}{C^2}}\right) \\ &= \frac{d_0}{2}\left(1 + \frac{1}{\sin\theta/2}\right). \end{aligned} \tag{2.18}$$

The classical scattering distance in relation to the minimum distance d_0 as function of the scattering angle is shown in Fig. 2.3.

2.2.3 Trajectories in the Point-Charge Coulomb Field

For the motion in a central-force field with a force $\propto r^{-2}$ classical mechanics shows that the trajectories are conic sections (for scattering, i.e. positive total energy, these are hyperbolae). To derive this one needs again the conservation laws of angular momentum and energy (with the Coulomb potential):

$$L = m r^2 \dot{\phi} = \text{const} \tag{2.19}$$

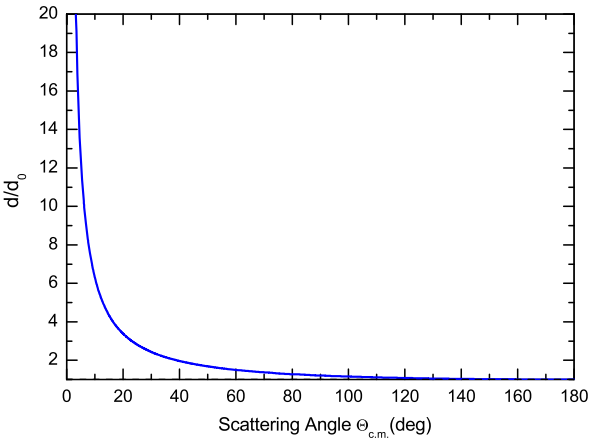

Fig. 2.3 Minimal scattering distance d (in units of d_0) as function of the c.m. scattering angle

$$E = \frac{mr^2}{2} + \frac{L^2}{2mr^2} + \frac{C}{r}. \tag{2.20}$$

In these equations dt can be eliminated. The integration of

$$d\phi = -\frac{L}{mr^2}\left[\frac{2}{m}\left(E - \frac{C}{r} - \frac{L^2}{2mr^2}\right)\right]^{-1/2} dr \tag{2.21}$$

results in

$$r = \frac{L^2}{mC} \cdot \frac{1}{1 - \epsilon\cos\phi} \tag{2.22}$$

with $b = L/\sqrt{2mE}$. With $k = L^2/mC$ and $\epsilon = \sqrt{1 + \frac{4E^2b^2}{C^2}}$ (the eccentricity) the standard form of conic sections is obtained

$$\frac{1}{r} = \frac{1}{k}(1 - \epsilon\cos\phi). \tag{2.23}$$

2.2.4 Consequences

There is now a connection between impact parameter b, scattering angle θ, and (quantized) orbital angular momentum $L = \ell\hbar$

$$b = \frac{1}{2}d_0 \cot\frac{\theta}{2} = \frac{\ell\hbar}{p_\infty}. \tag{2.24}$$

Because of the quantization of L the orbital angular-momentum quantum numbers $l = 0, 1, 2, \ldots$ correspond to annular zones around the z direction. Larger scattering angles belong to smaller impact parameters and smaller orbital angular momenta.

2.2.5 Consequences of the Rutherford Experiments and Their Historic Significance

Rutherford and his collaborators Geiger and Marsden (later also Chadwick) used α particles from radiactive sources as projectiles. Their energies were so small that for all scattering angles the minimum scattering distances d were large compared with the sum of the two nuclear radii of projectiles and targets. The complete agreement between the results of the measurements and the (point-)Rutherford scattering cross section formula shows this in accordance with Gauss's law of electrostatics, which can be used to prove that a finite charge distribution in the external space beyond the charges cannot be distinguished from a point charge with an r^{-1} potential. In addition, the mere occurrence of backward-angle scattering events proves uniquely by simple kinematics that the target nuclei were heavier than the projectiles. Thus the existence of the atomic nucleus as a compact (i.e. very small and heavy object) was established (and Thomson's idea of a "plum-pudding" of negative charges from distributed electrons, in which the positive charges of ions were suspended, was refuted).

The dependence of the Rutherford cross section on the atomic charge number Z has been used to check on the correct assignment of Z to chemical elements and their positioning in the periodic table—complementing the use of the characteristic X-ray spectra together with Moseley's law.

2.2.6 Quantum-Mechanical Derivation of Rutherford's Formula

The Rutherford cross section may be derived quantum-mechanically by solving the Schrödinger equation with the point (or extended) Coulomb potential as input and with suitable boundary conditions. This equation has the form of a hypergeometric differential equation.

$$-\frac{\hbar^2}{2\mu}u'' + \left(\frac{C}{r} + \frac{\hbar^2}{2\mu}\frac{\ell(\ell+1)}{r^2} - \frac{\hbar^2 k^2}{2\mu}\right)u = 0. \tag{2.25}$$

After decomposition into partial waves (with ℓ designating the angular momentum of each), this equation may be written in its "normal" form with the Sommerfeld parameter η_S, as defined in Eq. (2.2), and $\rho = kr$ with k the c.m. wave number of the projectile:

$$\frac{d^2 u_\ell(\rho)}{d\rho^2} + \left(1 - \frac{\ell(\ell+1)}{\rho^2} - 2\frac{\eta_S}{\rho}\right)u_\ell(\rho) = 0, \tag{2.26}$$

where $u_\ell(\rho)$ is the radial wave function solving the equation. *Asymptotically* the solutions are the regular and irregular Coulomb Functions with the Coulomb phases $\sigma_\ell = \arg\Gamma(\ell + 1 + i\eta_S)$:

$$F_\ell \longrightarrow \sin(kr - \ell\pi/2 - \eta_S \ln 2kr + \sigma_\ell), \tag{2.27}$$

$$G_\ell \longrightarrow \cos(kr - \ell\pi/2 - \eta_S \ln 2kr + \sigma_\ell). \tag{2.28}$$

With the usual partial-wave expansion with incident plane waves the Coulomb scattering amplitude of the outgoing wave results:

$$\Psi_S \longrightarrow \frac{1}{r} e^{i(kr - \eta_S \ln 2kr)} f_c(\theta), \tag{2.29}$$

$$f_c(\theta) = -\eta_S \frac{e^{2i\sigma_0} \cdot e^{i\eta_S \ln \sin^2 \theta/2}}{2k^2 \sin^2 \theta/2}. \tag{2.30}$$

The amplitude squared $f_C \cdot f_C^*$ provides the Rutherford cross section, which is identical to the classically derived equation. However, for all applications where there is interference the Rutherford amplitude has to be used including its (logarithmic) phase, responsible for the long range, and the s-wave Coulomb phase σ_0. Typical cases are that of identical particles (see Sect. 3.4) or of interference with nuclear (hadronic) amplitudes (see e.g. Sect. 7.2). In these cases the partial-wave expansion cannot be truncated at low partial waves.

2.2.7 Deviations from the Rutherford Formula

According to the previous discussion deviations from the point Rutherford cross section are expected in the following cases:

- Modifications of the point Coulomb potential by the screening effects of the atomic electrons, which must be described by a screened Coulomb potential. These effects should show up especially at forward angles. Details will be discussed below when the Rutherford cross section is derived using the Born approximation (Sect. 10.7).
- Extended charge distribution and sufficiently high incident energy such that the projectile "dives" into the nuclear volume. Leptonic projectiles can probe the charge distribution without interfering strong-interaction effects and with no volume of their own. For hadronic charged projectiles one expects strong effects from the nuclear interaction whereas neutrons see the matter-density distribution only. With many such scattering experiments, besides the different density distributions, charge and matter radii of the nuclei and nucleons and their systematics with the nuclear mass number A were determined (see below). This principle was also applied in the deep-inelastic scattering of very high-energy leptons (electrons, muons, and neutrinos) from nucleons, which led to the evidence of substructures (partons, which finally turned out to be the quarks) inside the nucleons and to the determination of all their properties such as spin, masses, charges etc.

2.3 Scattering, Density Distributions, and Nuclear Radii

2.3.1 Nuclear Radii from Deviations from Rutherford Scattering

Already without detailed knowledge of the density distribution and of the potential some quite precise statements about nuclear radii by scattering of charged projectiles from nuclei were possible. One condition for this is, however, that the potential, which is responsible for the deviations from the point cross section is of short range, i.e. the charge distribution has a relatively sharp edge.

Most impressively these deviations from the point cross section appear with diminishing distances between projectile and target in a suitable plot. Because the Rutherford cross section itself is strongly energy and angle dependent one may choose to plot the ratio

$$\left(\frac{d\sigma}{d\Omega}\right)_{\text{exp}} \Big/ \left(\frac{d\sigma}{d\Omega}\right)_{\text{point, theor.}} \tag{2.31}$$

as function of the minimum scattering distance d. Thus data at very different energies and angles can be directly compared (see Fig. 2.7 in Sect. 2.3.5). If, in addition, one wants to check on the assumption of the systematics of nuclear radii to follow $r = r_0 A^{1/3}$ a universal plot for all possible scattering partners by plotting the above ratio against $d/(A_1^{1/3} + A_2^{1/3})$ is useful. The experimental results show the extension of the charge distribution and the rather sudden onset of (hadronic) absorption (provided the interaction has a strong absorption term, which is typical for $A \geq 4$).

2.3.2 Coulomb Scattering from an Extended Charge Distribution

Here the quantum-mechanical derivation of the Rutherford-scattering cross section for a homogeneous charge distribution is useful. Starting points are

- Fermi's *Golden Rule* of perturbation theory.
- The first Born approximation.

For a "sufficiently weak" perturbation Fermi's *Golden Rule* gives the transition probability per unit time W:

$$\begin{aligned} W &= \frac{2\pi}{\hbar} \left|\langle \Psi_{\text{out}} | H_{\text{int}} | \Psi_{\text{in}} \rangle\right|^2 \rho(E) \\ &= \frac{V m p d\Omega}{4\pi^2 \hbar^4} \cdot |H_{if}|^2. \end{aligned} \tag{2.32}$$

The density of final states $\rho(E) = dn/dE$, which enters the calculation can be obtained from the ratio of the actual to the minimally allowed phase-space volumes:

$$\frac{dn}{dE} = \frac{V 4\pi p^2 dp \frac{d\Omega}{4\pi}}{(2\pi\hbar)^3 dE}, \tag{2.33}$$

$E = p^2/2m$ and $dp/dE = m/p = E/c^2 p$. Thus

$$\rho(E) = \frac{dn}{dE} = V\frac{pm d\Omega}{(2\pi\hbar)^3} = V\frac{pE d\Omega}{(2\pi\hbar)^3 c^2}. \tag{2.34}$$

W becomes the cross section according to the definition on p. 14 with the incident particle-current density $j = v/V = p/mV$:

$$d\sigma = \frac{W}{j} = \frac{W}{(\frac{p}{mV})} = \frac{V^2 m^2 d\Omega}{4\pi^2\hbar^4} \cdot |H_{if}|^2. \tag{2.35}$$

The 1st Born approximation consists in using only the first term of the Born series (see Sect. 10.7) with plane waves in the entrance and exit channels:

$$\Phi_{\text{in}} = \frac{1}{\sqrt{V}} e^{i\vec{k}_i\vec{r}} \quad \text{and} \quad \Phi_{\text{out}} = \frac{1}{\sqrt{V}} e^{i\vec{k}_f\vec{r}}. \tag{2.36}$$

If $H_{\text{int}} = U(r)$ signifies a small time-independent perturbation then, with $\vec{K} = \vec{k}_f - \vec{k}_i$

$$|H_{if}| = \left| \frac{1}{V} \int e^{i\vec{K}\vec{r}} U(r) d\tau \right| \tag{2.37}$$

and

$$\frac{d\sigma}{d\Omega} = \left(\frac{m}{2\pi\hbar^2}\right)^2 \left| \int e^{i\vec{K}\vec{r}} U(r) d\tau \right|^2 = \left| f(\theta) \right|^2. \tag{2.38}$$

Inserting the Coulomb potential $U(r) = C/r$ the classically calculated formula for the Rutherford scattering cross section is obtained. The cross section is (with the constant $Z_1 Z_2 e^2/16$ and the substitution $u = iKr\cos\theta$ and $du = -\sin\theta\, d\theta(iKr)$)

$$\begin{aligned}
\frac{d\sigma}{d\Omega} &= \text{const} \cdot \left| \int e^{i\vec{K}\vec{r}} \cdot \frac{1}{r} d\tau \right|^2 \\
&= \text{const} \cdot \left| \int\int \frac{1}{r} e^{iKr\cos\theta} 2\pi \sin\theta\, d\theta r^2 dr \right|^2 \\
&= \text{const} \cdot 2\pi \left| \int\int \frac{r}{iKr} e^u\, du\, dr \right|^2 \\
&= \text{const} \cdot \left(\frac{2\pi}{iK}\right)^2 \left| \int_r \left(e^{iKr\cos\pi} - e^{iKr\cos 0} \right) dr \right|^2 \\
&= \text{const} \cdot \left(\frac{2\pi}{iK}\right)^2 \left| \int_r \left(e^{-iKr} - e^{iKr} \right) dr \right|^2
\end{aligned}$$

$$= \text{const} \cdot \left(\frac{2\pi \cdot 2i}{iK} \right)^2 \left| \int_0^\infty \sin Kr \, dr \right|^2 . \tag{2.39}$$

The integral is undefined. This is circumvented by a *screening Ansatz* after Bohr, which corresponds to the real situation of the screening of the point Coulomb potential by the electrons of the atomic shell, with the screening constant α. With

$$\int_0^\infty e^{-\alpha r} \sin Kr dr = \frac{K}{K^2 + \alpha^2} \tag{2.40}$$

one obtains

$$\left(\frac{d\sigma}{d\Omega} \right)_{R,s} = \left[\frac{2\mu Z_1 Z_2 e^2}{\hbar^2 [\alpha^2 + 4k^2 \sin^2(\theta/2)]} \right]^2 \tag{2.41}$$

with the momentum transfer $K = 2k \sin(\theta/2)$ for elastic scattering. This cross section is finite for $\theta \to 0°$. By letting the screening constant go to zero a cross section results, which is identical with that from the classical derivation:

$$\begin{aligned} \left(\frac{d\sigma}{d\Omega} \right)_R &= \lim_{\alpha \to 0} \left(\frac{d\sigma}{d\Omega} \right)_{R,s} \\ &= \left(\frac{Z_1 Z_2 e^2}{4E_{\text{kin}}} \right)^2 \cdot \frac{1}{\sin^4(\theta/2)} . \end{aligned} \tag{2.42}$$

The extension of the derivation of the Rutherford cross section to an extended (especially a homogeneous and spherically-symmetric) charge distribution is simple and leads to the fundamental concept of the *form factor*. Such a distribution is suggested by the approximately constant nucleon density with r in most nuclei (see Fig. 2.8), but cannot represent the density behavior around R very well.

We start with the Coulomb potential of such an extended homogeneous spherical charge distribution with radius R (see Fig. 2.4). It is calculated with Gauss's theorem of electrostatics (for units see the footnote 2 in Sect. 2.2.) At $r = R$ the interior and exterior potential must be suitably matched.

$$V(r) = \begin{cases} ze^2 \frac{1}{r} & \text{for } r > R \\ ze^2 \frac{1}{2R} (3 - \frac{r^2}{R^2}) & \text{for } r \le R. \end{cases} \tag{2.43}$$

In the exterior space the potential is identical with that of a point charge, continues at $r = R$ to a parabolic shape in the interior of the distribution. It is therefore to be expected that in the scattering with sufficiently high energy the scattering cross section would strongly deviate from the Rutherford cross section as soon as the nuclear surface is touched. In addition, the onset of the short-range strong interaction will influence the scattering, especially by absorption. For the calculation of the cross section an integral over the contributions from all charge elements $dq = Ze\rho(\vec{r})d\tau$

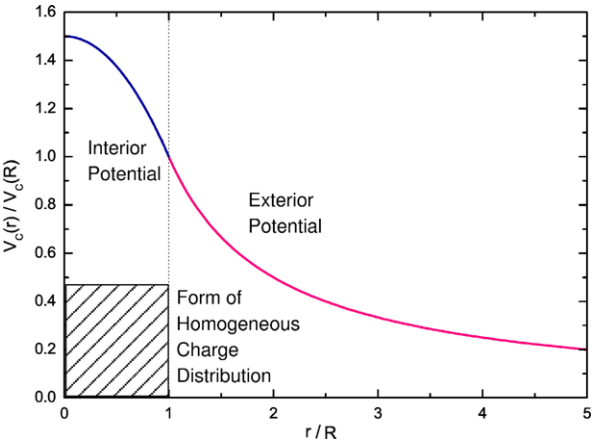

Fig. 2.4 Coulomb potential of a spherical homogeneous charge distribution in relation to the point-Coulomb potential that is valid outside the charge distribution, normalized to $V(r = R) = 1$

to the potential $U(\vec{r}) = -\frac{Z_1 Z_2 e^2}{R} \cdot e^{-\alpha R} \rho(\vec{r}) d\tau$ has to be performed.

$$U(\vec{r}') = -Z_1 Z_2 e^2 \int \rho(\vec{r}') \frac{e^{-\alpha R}}{R} d\tau. \tag{2.44}$$

By inserting this into the Born approximation Eq. (10.25) (with $d\vec{R} = d\vec{r}'$ and $\vec{R} = \vec{r}' - \vec{r}$) one obtains:

$$\begin{aligned} \frac{d\sigma}{d\Omega} &= \left(\frac{Z_1 Z_2 e^2 m}{2\pi\hbar^2} \right)^2 \cdot \left[\int \rho(\vec{r}) e^{i\vec{K}\vec{r}} d\tau \cdot \int \frac{e^{-\alpha R}}{R} e^{i\vec{K}\vec{R}} d\vec{R} \right]^2 \\ &= \left[F(\vec{K}^2) \frac{K}{K^2 + \alpha^2} \right]^2. \end{aligned} \tag{2.45}$$

The cross section factorizes into two parts, one of which (after a transition to the limit $\alpha \to 0$) results again in the point cross section, the other in the *form factor*:

$$\frac{d\sigma}{d\Omega} = \left(\frac{d\sigma}{d\Omega} \right)_{\text{point nucleus}} \cdot \left| F(\vec{K}^2) \right|^2. \tag{2.46}$$

This separation is characteristic for the interaction between extended objects and signifies a separation between the interaction (e.g. the Coulomb interaction) and the structure of the interacting particles.

For rotationally-symmetric problems the form factor has a simplified interpretation:

$$F(K) = \int \rho(r) \exp(i\vec{K}\vec{r}) 2\pi r^2 dr \sin\theta d\theta. \tag{2.47}$$

On substitution $u = iKr\cos\theta$ and $du = -iKr\sin\theta d\theta$ this becomes

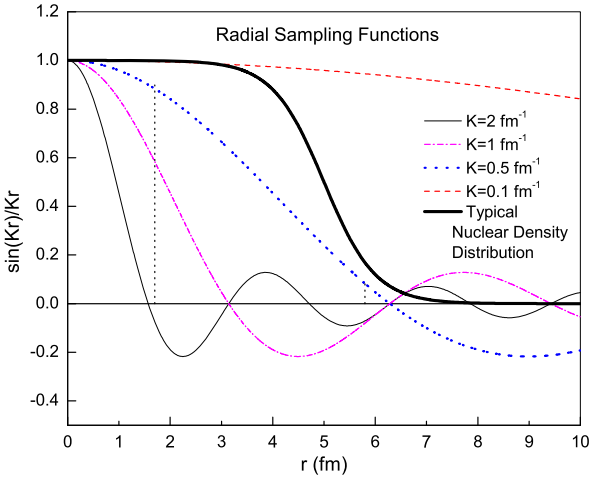

Fig. 2.5 Sampling functions for different momentum transfers show that in order to sample details of a given structure (e.g. the shape around the radius of a nuclear density (charge or mass) distribution) the momentum transfer (given by the incident energy and the scattering angle) has to have an appropriate intermediate value. In the example shown the value of $K = 0.5$ fm^{-1} is suitable for sampling the region around the nuclear radius of 5.0 fm. The *vertical dotted lines* indicate a 10 to 90 % sampling region

$$F(K) = 2\pi \int \rho(r) e^{u} r^2 dr \frac{du}{-iKr}$$
$$= \int \rho(r) 4\pi r^2 dr \cdot \underbrace{\left(\frac{\sin(Kr)}{Kr}\right)}_{\text{purely real}}. \tag{2.48}$$

Thus the form factor is a folding integral of the density with the sampling function (in parentheses). This function is oscillatory and its oscillation "wavelength" $1/K$ (which depends on the energy of the transferred radiation) has to be adjusted to the rate of change of the density. If the oscillation is too frequent the integral results in ≈ 0 revealing no information on ρ. If it is too slow the sampling function is $\approx$constant, and the integral results in just the total charge Ze. Figure 2.5 illustrates this for different momentum transfers on a given nuclear density distribution. Experimentally the form factor is obtained as the ratio

$$\left(\frac{d\sigma}{d\Omega}\right)_{\text{experimental}} \Big/ \left(\frac{d\sigma}{d\Omega}\right)_{\text{point, theor.}}. \tag{2.49}$$

The charge distribution (or more generally: the density distribution e.g. of the hadronic matter) is obtained by *Fourier inversion* of the form factor F:

$$\rho_c(\vec{r}) = \frac{1}{(2\pi)^3} \int_{0\to\infty} F_c\left(\vec{K}^2\right) e^{(-i\vec{K}\vec{r})} d\vec{K}. \tag{2.50}$$

This means that (in principle) for a complete knowledge of $\rho(\vec{r})$ F must be known for all values of the momentum transfer. Since $\rho(\vec{r})$ for small $\vec{r}$ is governed by the high-momentum transfer components of $\vec{K}$ this cannot be achieved in practice. For this reason the following approximations may be used:

- Model assumptions are made for the form of the distribution: e.g. homogeneously charged sphere, exponential, Yukawa, or Woods-Saxon behavior.
- The model-independent method of the expansion of $e^{i\vec{K}\vec{r}}$ into moments.

2.3.3 Ansatz for Models

It is useful to get an impression of the Fourier transformation of different model density-distributions as shown in Fig. 2.6: It is a general observation that "sharp-edged" distributions lead to oscillating form factors (and therefore cross sections), and smooth distributions to smooth form factors. In agreement with our Ansatz a δ distribution (characteristic for a point charge or mass) corresponds to a constant form factor (this is called "scale invariance").

2.3.4 Expansion into Moments

With the power-series expansion of $e^{i\vec{K}\vec{r}}$ the form factor becomes

$$F\left(\vec{K}^2\right) \propto \int \rho(\vec{r}) \left[1 + i\vec{K}\vec{r} - \frac{(\vec{K}\vec{r})^2}{2!} \pm \cdots\right] d\tau. \tag{2.51}$$

By assuming a spherically symmetric distribution (with pure r dependence only) and with a normalization such that for a point object the constant form factor is 1, we have:

$$F\left(\vec{K}^2\right) = 1 - \text{const} \cdot K^2 \int_{0\to\infty} r^2 \rho(r) d\tau \pm \cdots. \tag{2.52}$$

The second term contains the average squared radius $\langle r^2 \rangle = r_{rms}^2$. For small values of $K^2\langle r^2\rangle$ one gets in a model-independent way (i.e. for arbitrary form factors):

$$F\left(\vec{K}^2\right) \approx 1 - \frac{1}{6} K^2 \langle r^2 \rangle. \tag{2.53}$$

Of course this approximation is becoming worse with smaller r (because one needs higher moments), i.e. if one wants to resolve finer structures.

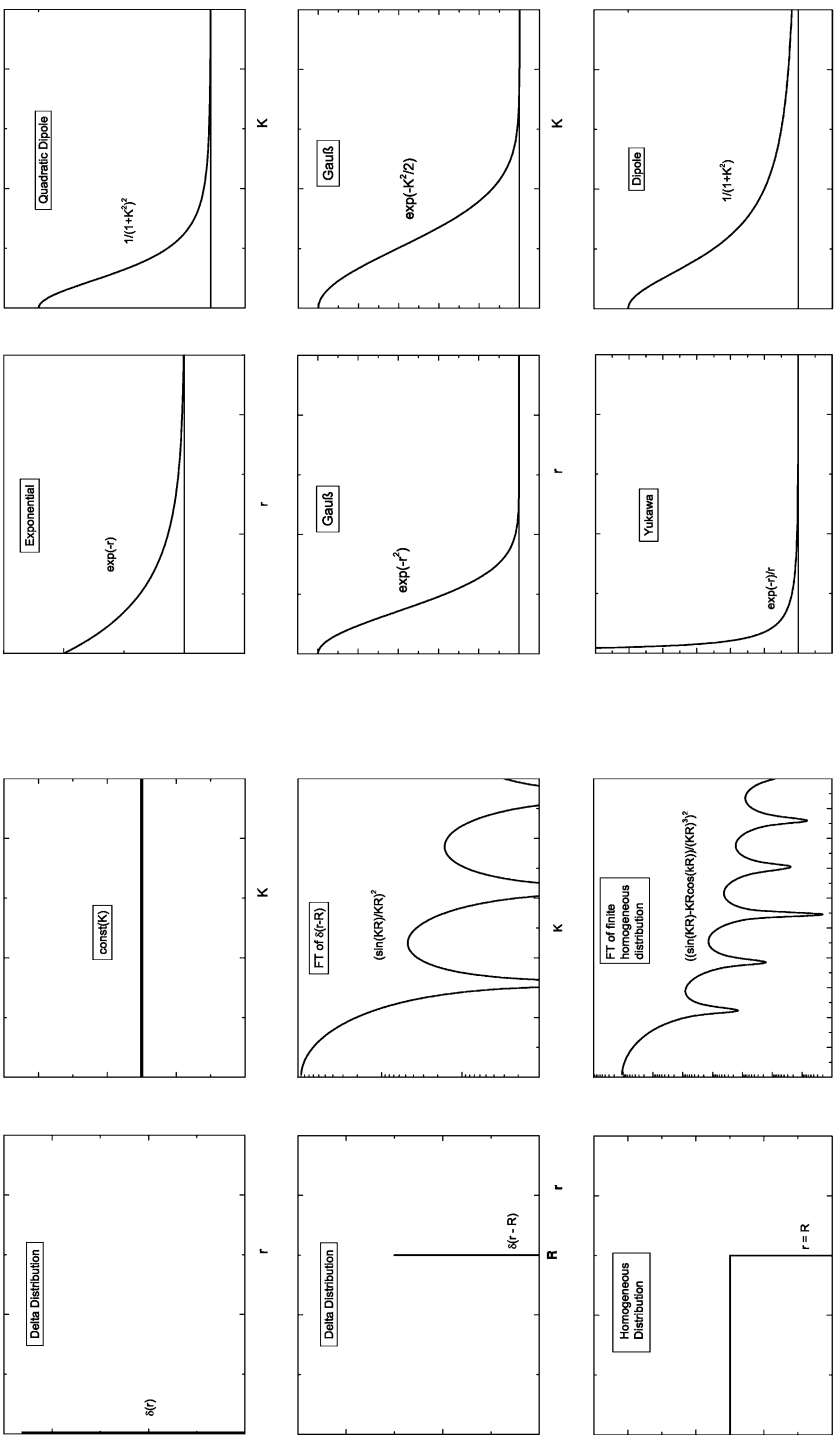

Fig. 2.6 *Squares* of the Fourier transforms—basically the form factors determining the shapes of the cross sections—of different charge-density distributions

2.3.5 Results of Hadron Scattering

After accelerators were available charge and matter density distributions of nuclei and their radii could be investigated by probing the distributions with hadronic projectiles. With light as well as with heavy ions, but also with neutrons as projectiles it is evident that they are extended and possess structure. The consequence is that detailed statements about the density distributions are difficult to make and may need the deconvolution of the contributions from projectile and target nuclei. However, statements about nuclear radii are possible, even with quite simple semi-classical assumptions such as absorption between nuclei setting in sharply at a well-defined distance and pue Coulomb scattering beyond that distance. Systematic α scattering studies on many nuclei (where we already have strong absorption at the nuclear surfaces) revealed good $A^{1/3}$ systematics for the nuclear radii. A dependence of

$$\sigma_{\alpha,\alpha} = R_0\left(A^{1/3} + 4^{1/3}\right) \tag{2.54}$$

was fitted to the data, assuming a sharp-cutoff model for the cross sections and taking into account the finite radii of both nuclei. It yielded a radius constant of

$$R_0 = 1.414 \text{ fm}. \tag{2.55}$$

However, when considering the range of the nuclear force for both nuclei of about 1.4 fm a radius constant of $\approx$1.2 fm resulted.

Heavy-ion scattering experiments with a great number of different pairs of collision partners yielded a very good systematics shown in Fig. 2.7 that becomes evident when the relative cross sections were plotted against the distance parameter d, for which an assumed $A^{1/3}$ dependence of the radii of both collision partners was applied

$$d = D_0\left(A_1^{1/3} + A_2^{1/3}\right)^{-1} \tag{2.56}$$

with D_0 the distance of closest approach, as calculated from energies and scattering angles. A well-defined sharp distance parameter of $d_0 = 1.49$ fm for the onset of absorption resulted. This corresponds to a universal radius parameter of $r_0 = 1.1$ fm if the range of the nuclear force is set to 1.5 fm. The simple model applied was to assume

- Pure point-Rutherford scattering outside the range of nuclear forces,
- Ratio of elastic to Rutherford cross section

$$\frac{d\sigma}{d\sigma_R} = 1 + P_{\text{abs}}(D) \tag{2.57}$$

and

$$P_{\text{abs}}(D) = \begin{cases} 0 & \text{for } D \geq D_0, \\ 1 - \exp(\frac{D-D_0}{\Delta}) & \text{for } D < D_0, \end{cases} \tag{2.58}$$

with $P_{\text{abs}}(D)$ the probability of absorption out of the elastic channel, D_0 the interaction distance, and Δ the "thickness" of the transition region.

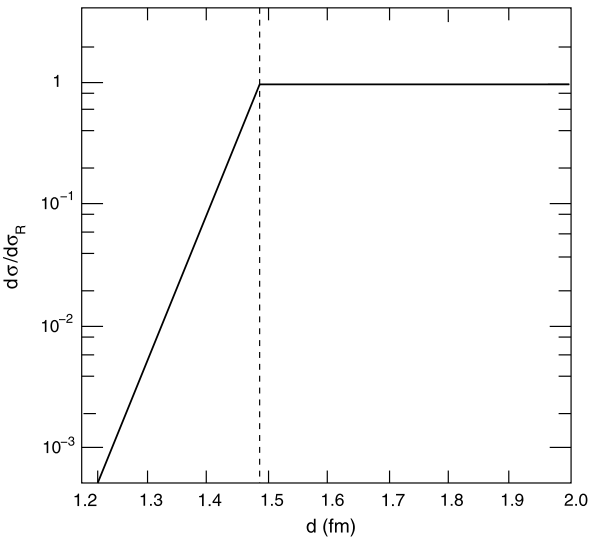

Fig. 2.7 Plot of the scattering cross sections (relative to the Rutherford cross section) of many different HI pairings vs. the distance parameter d in fm. The data used for the fit are in Ref. [OGA78], see also [CHR73]

The latter depends on the A of the nuclei involved and could be determined with good accuracy to be e.g. $\Delta \approx 0.33$ fm for scattering of nuclei near ^{40}Ca from ^{208}Pb.

Here we will discuss the results obtained with charged projectiles, for which the interaction is exactly known (e.g. electrons, which do not interact via the strong force) whereas e.g. for neutrons one needs nuclear scattering models (e.g. the optical model, see Sect. 10.3). The assumption that neutron and proton radii of nuclei are about equal has proved too simple with the evidence of neutron-halo and neutron-skin nuclei, see Sect. 2.4.2.

2.4 Electron Scattering

Since all electrons (and all leptons) are considered to be point-particles they are—as long as not the hadronic interaction region proper shall be probed—the ideal projectiles. They "see" the electromagnetic (and weak) structure of the nuclei. Of course, the treatment must be relativistic. Instead of the Rutherford- (point-Coulomb) approach one has to use the proper theory.

Besides the relativistic treatment differences to the (classical) Rutherford cross section come about by the lepton spin. The derivation of the correct scattering cross section relies on the methods of Quantum Electrodynamics (QED) and techniques such as the Feynman diagrams. Here only the results will be presented. The electromagnetic interaction between the electron and a hadron is mediated by the exchange of virtual photons, which is accompanied by a transfer of energy and momentum. The wavelength of these photons derives directly from the momentum

transfer $\hbar K = 2(h\nu/c)\sin(\theta/2)$ to be

$$\lambda\!\!\!^{-}_{\text{de Broglie}} = \frac{\hbar}{\hbar K} = 1/K. \tag{2.59}$$

The argument of diffraction limitation may also be formulated in the complementary time picture; it may be said that at long wavelengths, due to the uncertainty relation, one needs long measurement times, in which the projectile sees only a time-averaged picture of the object considered while small wavelengths allow measurement times equivalent to snapshots of the object or its substructures (partons).

In contrast to low-energy Rutherford scattering, in which only the electric charges interact, in charged lepton scattering at higher (relativistic) energies there is also a magnetic interaction, and in neutrino scattering only the weak interaction is acting. Principally in lepton scattering at higher energies three distinct regions of momentum transfer can be distinguished:

- Elastic scattering at small momentum transfer is suitable to probe the shape of the hadrons. The resulting two form factors F_E (electric) and F_M (magnetic) produce again the charges and current (magnetic moment) distributions and the radii of the hadrons by Fourier inversion.
- Weakly inelastic scattering at higher momentum transfer leads to excitations of the hadrons (e.g. Delta- or Roper excitations (resonances) of the nucleons). The form factors are quite similar to those from the elastic scattering, which means that we have some excited state of the same nucleons.
- Deep-inelastic scattering is the suitable method to see partons inside the hadrons. In this way in electron and muon scattering the quarks bound in nucleons and their properties (spin, momentum fraction) and also the existence of sea quarks (s quark/anti-quark pairs) were identified. Especially the pointlike character of these constituents was shown by the near constancy of the form factors (here called: *structure functions*) with the momentum transfer (*Bjorken scaling*).

Here only elastic scattering will be discussed in detail. In QED theory for the differential cross section the Rosenbluth formula was deduced:

$$\frac{d\sigma}{d\Omega} = \left(\frac{d\sigma}{d\Omega}\right)_{\text{point}} \cdot \left(\frac{F_E^2 + bF_M^2}{1+b} + 2bF_M^2 \tan^2\frac{\theta}{2}\right). \tag{2.60}$$

The point cross section $(d\sigma/d\Omega)_{\text{point}}$ is a generalized Rutherford cross section and is calculable with the methods of QED (e.g. using Feynman diagrams). The most general form of this cross section (the Dirac scattering cross section) contains as main part the electrostatic scattering, a contribution from the magnetic (spin-dependent) interaction, which depends on the momentum transfer, and a correction for the nuclear recoil:

$$\left(\frac{d\sigma}{d\Omega}\right)_{\text{Dirac}} = \frac{\alpha^2}{4p_0^2\sin^4(\theta/2)}\left[1 + \frac{2p_0}{M}\sin^2\frac{\theta}{2}\right]\left(\cos^2\frac{\theta}{2} + \frac{q^2}{2M^2}\sin^2\frac{\theta}{2}\right). \tag{2.61}$$

For small energies or momentum transfers the cross section simplifies to:

$$\left(\frac{d\sigma}{d\Omega}\right)_{\text{Mott}} = \frac{[2e^2(E'c^2)]^2}{q^4} \cdot \frac{E'}{E} \cos^2 \frac{\theta}{2}. \tag{2.62}$$

The symbols used here mean: q = four-momentum transfer, $b = -q^2/(4m^2c^2)$, E', and E the energies of the outgoing and incoming electrons. F_E and F_M are the electric and magnetic form factors of the nucleons. Experimentally they are obtained from the measured data by least-squares fitting of the parameters of the theory, graphically through the *Rosenbluth plot*, i.e. by plotting $(d\sigma/d\Omega)_{\text{exp}}/(d\sigma/d\Omega)_{\text{point}}$ against $\tan^2(\theta/2)$.

In analogy to the Rutherford cross section here the form factors (or structure functions) are Fourier transforms of the charge and current-density distributions (or: distributions of the (anomalous) magnetic moments). Like there, these distributions result from Fourier inversion of the form factors, and at the same time quantitative values of the shape and size of the nucleons are obtained.

The measured form factors as functions of q^2 are normalized such that for $q \to 0$ they become the static values of the electric charge and magnetic moments. Except for the electric form factor of the neutron all others are well described by the dipole Ansatz corresponding to a density distribution of an exponential function.

An early model for the charge-density distribution was—besides the homogeneously charged sphere with only one parameter, its radius—a modified Woods-Saxon distribution with three parameters, because, besides the radius parameter r_0 and the surface thickness a, also the central density ρ_0 must be adjustable because it varies especially in light nuclei:

$$\rho_c(r) = \frac{\rho_0}{1 + e^{\frac{r - r_{1/2}}{a}}}. \tag{2.63}$$

The surface thickness $t = 4 \ln 3 \cdot a$ signifies the 10 to 90 % thickness range centered around $r_{1/2}$. From this parametrization an electromagnetic radius constant of $r_{1/2} = 1.07$ fm, a surface-thickness parameter of $a = 0.545$ fm, and a central density of $\rho_N = 0.17$ nucleons/fm^3 or $1.4 \cdot 10^{14}$ g/cm^3 for nuclei with $A > 30$ have been derived. The description of "modern" density distributions is not so simple because the nuclei have individual and more complex structure even if the essential features such as the three parameters do not vary too much. The detailed structure information is obtained from model-independent approaches such as Fourier-Bessel expansions. Radii are given as rms radii or converted into the equivalent radii R_0. R_0 is the radius of a homogeneously charged sphere of equal charge using the relation

$$r_{\text{rms}} = \sqrt{3/5} R_0. \tag{2.64}$$

The definition of the (model-independent) Coulomb rms radius is

$$r_{\text{rms}} = \langle r^2 \rangle^{1/2} = \left[\frac{1}{Ze} \int_0^\infty r^2 \rho_C(r) 4\pi r^2 dr \right]^{1/2}. \tag{2.65}$$

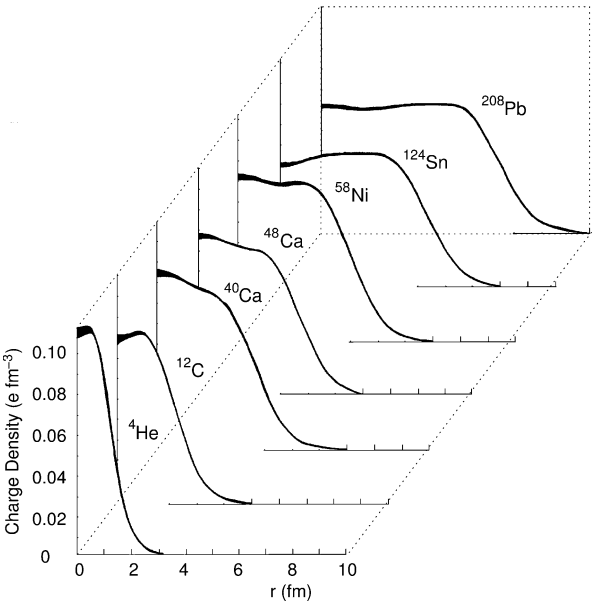

Fig. 2.8 Charge density distributions of different doubly closed-shell nuclei. The central density is only weakly changing over the nuclear chart whereas the radii increase with $A^{1/3}$. After [FRO87]

Nuclear radii from muonic atoms are often more precise than those from lepton scattering but they are in a way complementary in relation to the radius region probed they measure different moments). Thus, the results of both methods can be combined (Fig. 2.8). The distributions are quite well reproduced by "mean-field" calculations, see e.g. [FRO87, DEC68]. The salient results of these investigations are:

- From the distributions a central density is derived, which for heavier nuclei is constant in first approximation. This and the systematics of radii are characteristic for nuclear forces; their properties are: short range, saturation and incompressibility of nuclear matter, and suggest the analogy to the behavior of liquids, which led to the development of collective nuclear models (liquid-drop models, models of nuclear rotation and vibration).
- The radii follow more or less a simple law $r = R_0 A^{\frac{1}{3}}$. For the radius parameter $R_0 = 1.24$ fm is a good value. From Coulomb-energy differences of mirror nuclei a value of $R_0 = (1.22 \pm 0.05)$ fm has been derived.
- The surface thickness of all nuclei is nearly constant with a 10–90 % value of $t = 2.31$ fm corresponding to $a = t/4\ln 3 = 0.53$ fm. This is explained by the range of the nuclear forces independent of the nuclear mass number A.
- The nucleons have no nuclear surface. The charge and current as well as the matter densities of the proton follow essentially an exponential distribution. For the neutron the charge distribution is more complicated because volumes of negative and positive charges must compensate each other to zero notwithstanding some complicated internal charge distribution that originates from its internal quark-gluon structure.

- The rms radii for the current distributions of protons and neutrons and the charge distribution of the protons are 0.88 fm. Recently, with increased experimental precision an unresolved discrepancy between values from lepton scattering and muonic-atom work has been published. The rms charge radius of the neutron it is 0.12 fm, which means that there must be positive and negative charges distributed differently over the nuclear volume.
- Thus, nucleons are not "elementary", but have complicated internal structures.

2.4.1 Matter-Density Distributions and Radii

The matter density—apart from and independent of the charge or current distributions—can be investigated only by additional hadronic scattering experiments because neutrons and protons in principle need not have the same distributions in nuclei.

Hadronic Radii from Neutron Scattering The total cross sections of 14 MeV neutron scattering under simple assumptions have been shown to also follow a $A^{1/3}$ law, see e.g. Ref. [SAT90], p. 32, cited from Ref. [ENG74]. The assumptions were that the sharp-edged range of the nuclear force was 1.2 fm and the total cross section σ_{tot} follows $2\pi(R + \lambda\!\!\!^{-})^2$ with R the nuclear (hadronic) radius, i.e. the nuclei are considered to be black (totally absorbent) to these neutrons, which is not exactly fulfilled, as the structures in this dependence show. These can be explained with the optical model, see below. The radius constant extracted from this systematics is

$$R_{\text{hadr}} = 1.4 \text{ fm}. \tag{2.66}$$

In addition, there have been attempts to extract the neutron radius of ^{208}Pb from parity-violating electron scattering [ABR12].

2.4.2 Special Cases—Neutron Skins and Halo Nuclei

Neutron Skins Different from halos skins are a volume effect expected and appearing in heavier nuclei with increasing neutron excess (and densities over proton densities). The question of a neutron skin in these nuclei is interesting, and only recently such a thin skin was consistently shown to exist, see e.g. [TSA12] and references therein. Among the hadronic probes used have been protons, α's, heavy ions, antiprotons, and, recently, also pions e.g. on ^{208}Pb, ^{48}Ca and others. The extraction of rms radii requires some model assumptions concerning the reaction mechanism and the interplay of hadronic and Coulomb interactions. The pion results are derived from two sources: pionic atoms (in analogy to the derivation of the electromagnetic radii from muonic atoms) and total reaction cross sections of π^+ [FRI12].

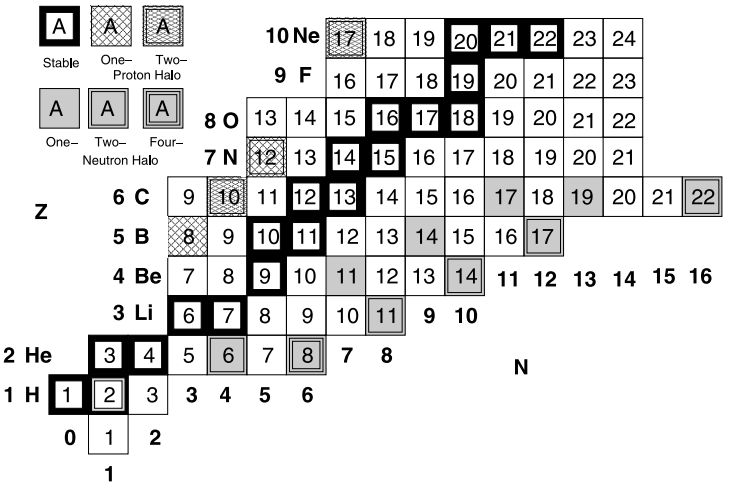

Fig. 2.9 Halo nuclei at the driplines of the chart of nuclides

The neutron skin is related to the symmetry energy, which plays a role in the mass formula of Bethe and Weizsäcker for the binding energies of nuclei, especially for "asymmetric" nuclei with strong neutron excess, but also for astrophysics and nuclear-matter calculations. The radius of neutron stars is closely related to the symmetry energy value in high-density nuclear matter, see e.g. Ref. [TSA12].

Usually the quantity

$$\delta R_{np} = \langle r^2 \rangle_n^{1/2} - \langle r^2 \rangle_p^{1/2} \tag{2.67}$$

is taken as a measure of skin thickness. The experimental values deduced from different experiments are on the order of $\delta R_{np} \approx 0.2$ fm.

Halo Nuclei At the "rims" of the valley of stability (the neutron or proton *driplines*) there are a number of nuclei that have much larger radii than expected from the systematics. ^{11}B has about the same radius as ^{208}Pb. Also the deuteron has an rms radius of about 3.4 fm. In all cases the nuclei seem to have a halo of weakly bound neutrons (or protons), which surrounds a more strongly bound core. Different cores are possible, i.e. besides the strongly bound α making ^{6}He and ^{8}He one- and two-neutron halo nuclei and ^{8}B and ^{10}C seem to form one- and two-proton halos, also ^{9}Be forms some type of core. Indications of halo structures were—among others—the exceptionally large cross sections in heavy-ion reactions, a narrower momentum distribution of the nucleons in the nuclei, and larger radii, as compared to the $A^{1/3}$ law. Figure 2.9 shows the low-mass portion of the chart of nuclides where halo nuclei have been found. The scientific interest in halo nuclei is manifold. They were among the first where the driplines have been reached. The results show that the shell structures established for the valley of stability can be extended to "exotic" nuclei, but with modifications of the closed shells, i.e. with new magic

Fig. 2.10 Coat of arms and symbol of the Renaissance Borromean family (and other north Italian families like the Sforzas) at their castle on the Borromean island Isola Bella in the Lago Maggiore, Italy

numbers emerging. The low mass numbers invite application of microscopic theories such as Faddeev-(Yakubowsky), no-core shell models, Green's function Monte Carlo (GFMC), and other approaches to test nuclear forces, e.g. three-body forces, or effective-field (EFT) approaches. Impressive results have been obtained by such "ab initio" calculations, see e.g. Ref. [PIE01, DEA07]. A special role is played by the so-called *Borromean* nuclei, i.e. those that consist of a core plus two weakly (un)bound neutrons at large radii, and for which any of the two-particle subsystems are unbound (Example: $^4\mathrm{He}+n+n$). They can be treated by well-established three-body methods; see also Chap. 9.2. Their name is derived from the three intertwined Borromean rings that fall apart when one ring is removed and hold together only when united, see Fig. 2.10. Many nucleosynthesis processes pass through nuclei that are neutron rich or neutron poor and are not well known. Thus, for astrophysics, a better understanding of all these reactions and their reaction rates is essential.

Since we deal with unstable (radioactive) nuclei the "radioactive-ion beams (RIB)" facilities, many of which are being developed, are especially suited for their investigation (for details see Chap. 15). These facilities collect, focus and accelerate nuclear reaction products in order to use them as projectiles in reactions. Figures 2.11 and 2.12 show the properties typical for halo nuclei:

- They have radii, which are larger than predicted from the usual $A^{1/3}$ systematics.
- Their density distributions reach further out than usual.
- In agreement with this they show narrower momentum distributions of the breakup fragments of the halo nuclei (one example: $^{19}\mathrm{C} \rightarrow {}^{18}\mathrm{C}+n$, compared to $^{17}\mathrm{C} \rightarrow {}^{16}\mathrm{C}+n$).
- The halo structure has to be distinguished from a neutron skin structure (see the preceding subsection). The latter is a volume effect caused by the increasing numbers of neutrons over protons with increasing A, whereas in light nuclei,

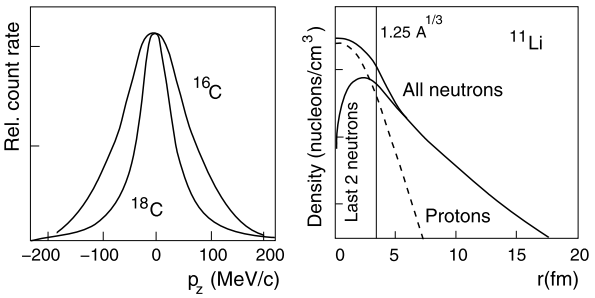

Fig. 2.11 Schematic fragment-momentum distributions from breakup reactions (*left*) and density distributions in halo nuclei, see e.g. Ref. [DOB06]

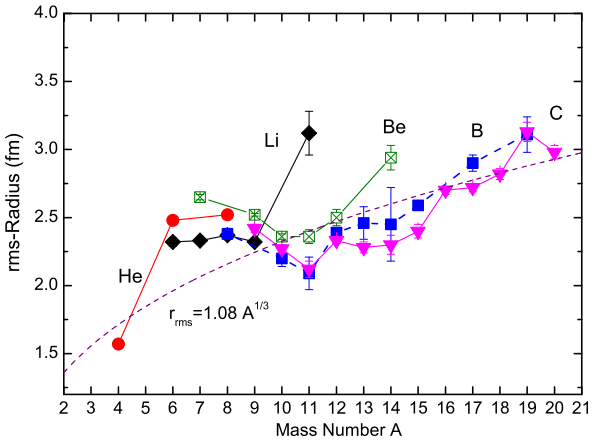

Fig. 2.12 Radii of halo nuclei. There exist (slightly varying, depending on extraction methods from experiments) numbers from different sources, especially from the earliest systematics from Ref. [TAN85]. Here they were taken from Refs. [OZA01] and [KRI12]. For comparison a plausible rms radius function for "normal" nuclei is shown

in approaching the n (or p) driplines, the binding energy of additional neutrons (or protons) approaches zero, making the nuclei nearly unbound which results in large radii.

The latest discovery at present of a halo nucleus is that of ^{22}C [TAN10] which showed an increased reaction cross section and an rms radius of $r_{\mathrm{rms}} = 5.4 \pm 0.9$ fm, both larger than expected from the usual systematics.

2.5 Exercises

2.1. (a) Show how kinematical arguments lead to Rutherford's conclusions on a (compact and) heavy target nucleus (gold).
(b) In the semi-classical theory of Bethe and Bloch (see Eq. (17.1)) the slowing-down of charged particles is explained with their being scattered by atomic electrons. What is different and what are the consequences from kinematics in this case: effects on the α projectiles and on the recoils electrons?

2.2. The "first" artificial nuclear reaction induced by an accelerated beam (Cockroft/Walton, 1932) was $^{7}_{3}\mathrm{Li}(p,\alpha)^{4}_{2}\mathrm{He}$ at an incident energy of 150 keV.

(a) Calculate the Q value of the reaction from the known masses of the particles (p: 1.007289 u, α: 4.002425 u, and $^{7}_{3}$Li: 7.014907 u).
(b) What are the energies of the two α's under the lab. angles of 0° and 90°?
(c) Does the *inverse*, i.e. time-reversed reaction have an energy threshold, and at which α lab. energy?

2.3. Chadwick discovered the neutron in 1932 by correctly identifying the energetic radiation emitted from the reaction $\alpha + {}^{9}_{4}\mathrm{Be} \rightarrow {}^{12}_{6}\mathrm{C} + {}^{1}_{0}n$ (induced by α's from a Po source). The recoil energies transferred to the protons and ^{14}N nuclei of the filling gas of the ionization chamber were measured to be 5.7 MeV and 1.6 MeV, respectively (masses: $^{9}_{4}$Be: 9.011348 MeV; ^{14}N: 14.002863 u).

(a) Which value of the neutron mass (in u) was obtained by Chadwick?
(b) Other nuclear physicists (among them the Curies) had erroneously interpreted the energetic radiation as γ radiation. How high would their energy have to be if they had transferred their energy by elastic Compton scattering (see Eq. (17.7)) on the protons or ^{14}N nuclei? Could such energies of γ transitions occur in nuclei?
(c) What exactly is their error of reasoning?

2.4. An $^{16}_{8}$O nucleus is scattered elastically at 80 MeV and 150° from a $^{179}_{79}$Au nucleus at rest in the lab. system.

(a) How close to each other (in a semi-classical picture) do the centers of the two nuclei get?
(b) Do the two nuclei "feel" the (hadronic) nuclear force, if a radius constant $R_0 = 1.25$ fm and as range of the force the value resulting from pion exchange + Heisenberg's uncertainty relation are assumed?

2.5. To resolve substructures ("partons") in nuclei (or nucleons), e.g. by elastic electron scattering the wavelength of the probing radiation must be chosen sufficiently small, more precisely: the wavelength of the exchanged (virtual) radiation.

(a) What electron energy is required to probe the surface of a $^{208}_{82}$Pb nucleus, of a ^{4}He nucleus, the rms-radius range of a proton, or quark structures inside nucleons in the $\leq 1 \cdot 10^{18}$ m range?
(b) What about using muons?

References

[ABR12] S. Abrahamyian et al. (PREX Collaboration), Phys. Rev. Lett. **108**, 112502 (2012)
[CHR73] P.R. Christensen, V.I. Manko, F.D. Becchetti, R.J. Nickles, Nucl. Phys. A **207**, 33 (1973)
[DEA07] D.J. Dean, Phys. Today. **November**, 48 (2007)
[DEC68] J. Dechargé, D. Cogny, Phys. Rev. C **21**, 1568 (1968)
[DOB06] A.V. Dobrovolsky et al., Nucl. Phys. A **766**, 1 (2006)

[ENG74] J.B.A. England, *Techniques in Nuclear Structure Physics* (Halstead, New York, 1974)
[FRI12] E. Friedman, Nucl. Phys. A **896**, 46 (2012)
[FRO87] B. Frois, C.N. Papanicolas, Annu. Rev. Nucl. Part. Sci. **37**, 133 (1987)
[GEI13] H. Geiger, E. Marsden, Philos. Mag. **25**, 604 (1913)
[KRI12] A. Krieger et al., Phys. Rev. Lett. **108**, 142501 (2012)
[NOE76] W. Nörenberg, H.A. Weidenmüller, *Introd. Theory of Heavy Ion Collisions*. Lecture Notes in Physics, vol. 51 (Springer, Heidelberg, 1976)
[OGA78] Y.T. Oganessian, Y.E. Penionzhkevich, V.I. Man'ko, V.N. Polyansky, Nucl. Phys. A **303**, 259 (1973)
[OZA01] A. Ozawa, T. Suzuki, I. Tanihata, Nucl. Phys. A **693**, 32 (2001)
[PIE01] S.C. Pieper, R.B. Wiringa, Annu. Rev. Nucl. Part. Sci. **51**, 53 (2001)
[SAT90] G.R. Satchler, *Introd. Nucl. Reactions*, 2nd edn. (McMillan, London, 1990)
[TAN85] I. Tanihata, H. Hamagaki, O. Hashimoto, Y. Shida, N. Yoshikawa, K. Sugimoto, O. Yamakawa, T. Kobayashi, N. Takahashi, Phys. Rev. Lett. **55**, 2676 (1985)
[TAN10] K. Tanaka et al., Phys. Rev. Lett. **104**, 062701 (2010)
[TSA12] M.B. Tsang, J.R. Stone, F. Camera, P. Danielewicz, S. Gandolfi, K. Hebeler, C.J. Horowitz, J. Lee, W.G. Lynch, Z. Kohley, R. Lemmon, P. Möller, T. Murakami, S. Riordan, X. Roca-Maza, F. Sammarrucca, A.W. Steiner, I. Vidaña, S.J. Yennello, Phys. Rev. C **86**, 015803 (2012)

http://www.springer.com/978-3-642-53985-5

Nuclear Reactions
An Introduction
Paetz gen. Schieck, H.
2014, XXV, 365 p. 184 illus., 87 illus. in color., Softcover
ISBN: 978-3-642-53985-5